

Acoustic Scattered Field Computation

C. Nguon, N. Nagadewate, K. Chandra and C. Thompson
Center for Advanced Computation and Telecommunications
Department of Electrical and Computer Engineering
University of Massachusetts Lowell
Lowell, MA. 01854

ABSTRACT

The scattering due to the interaction of dual-frequency beams on a three-dimensional object is considered. The difference-frequency generated from this interaction has the potential to improve the classification of biological tissue. This work examines the effect of the contrast parameter on the scattered field produced from an ellipsoidal scatterer.

1 Introduction

In 1963, Ingard and Pridmore-Brown [5] observed the generation of sum and difference frequencies from the intersection of two perpendicular plane waves in air. Darvennes and Hamilton [3] extended this work to calculate the difference-frequency sound outside the interaction region of two intersecting Gaussian beams. Their work determined that the scattering from the difference frequency depended on the frequency ratio, intersection angle, and source separation of the incident beams. Thierman [8] conducted experimental and computational work observing the difference-frequency signal produced from the interaction of focused beams on various targets. For the experimental setup and parameters chosen, Thierman was unable to measure any

detectable difference-frequency sound. Regardless, he still considered the possibility of producing a response from the interaction of dual-frequency pressures prompting for more analysis on the conditions behind difference-frequency sound.

The difference-frequency field arises from the nonlinearity of the medium in response to a high intensity incident pressure. The difference of two high frequency incident beams generate a low frequency signal that can better capture the acoustic features of the medium interrogated. This particular signal is of interest in providing an increased penetration depth [4][7]. The application of high frequency incident fields allows focusing and improved resolution of the tissue.

In this work, a computational model is presented for the solution of the forward scattered field due to the difference frequency component. This is undertaken by first solving for the first order pressure fields P_1 in the linearized wave equation due to the dual frequency field. The difference frequency component generated from this solution, being localized within the medium is then applied as a source term P_1^2 in the second order wave equation for far-field observations of the scattered pressure P_2 . The source term is weighted by the nonlinear parameter B/A which determines the influence of the difference frequency component. This nonlinear parameter B/A

characterizes the variation of the sound speed within the medium.

In Section 2, the governing equations for the first and second order pressure fields are presented. Section 3 describes the computational model. Section 4 presents results for scattering from an inviscid fluid ellipsoidal shaped scatterer for varying compressibility contrast parameters.

2 Scattering from Inhomogeneous Media

Consider a confocal transducer emitting dual-frequencies ω_a and ω_b onto a volume Ω surrounding an ellipsoid scattering region Ω_s . The incident field is represented as $P_i(\underline{x}, t) = \text{Re} [P_{ia}(\underline{x})^{(+)} e^{j\omega_a t} + P_{ib}(\underline{x})^{(+)} e^{j\omega_b t}]$ where P_{ia}^+ and P_{ib}^+ represent the incident pressure amplitudes. When the incident field ensonifies the scattering volume, the compressibility contrast $\epsilon = (\kappa_s - \kappa)/\kappa$ cause the waves to scatter.

To obtain an expression for the difference-frequency field, an expansion in pressure $P = P_0 + P_1 + P_2 + \dots$, density $\rho = \rho_0 + \rho_1 + \rho_2 + \dots$, and velocity $u = u_0 + u_1 + u_2 + \dots$ is applied to the governing equations of motion. By retaining terms to the first-order, the first-order inhomogeneous wave equation is expressed as,

$$\begin{aligned} \nabla^2 P_{1s}(\underline{x}, t) - \frac{1}{c_0^2} \frac{\partial^2}{\partial t^2} P_{1s}(\underline{x}, t) \\ = \epsilon \gamma_\kappa(\underline{x}) \frac{1}{c_0^2} \frac{\partial^2}{\partial t^2} P_{1s}(\underline{x}, t) \end{aligned} \quad (1)$$

for $s = a, b$, where c_0 is the speed of sound and $\gamma_\kappa(\underline{x})$ represents the region where ϵ is nonzero. Converting the first-order wave equation to the frequency domain, Eqn. (1) can be mapped to the Kirchhoff-Helmholtz equation,

$$\begin{aligned} P_{1s}(\underline{x}) = P_{is}(\underline{x}) \\ + \epsilon k_{1s}^2 \int_{\Omega_s} \gamma_\kappa(\underline{x}_0) P_{1s}(\underline{x}_0) G(\underline{x}, \underline{x}_0) d\underline{x}_0 \end{aligned} \quad (2)$$

for $s = a, b$, where $k_{1s} = \omega_s/c_0$ is the wavenumber and $G(\underline{x}, \underline{x}_0)$ is the three-dimensional free-space Green's function,

$$G(\underline{x}, \underline{x}_0) = \frac{e^{jk_{1s}|\underline{x}-\underline{x}_0|}}{4\pi|\underline{x}-\underline{x}_0|} \quad (3)$$

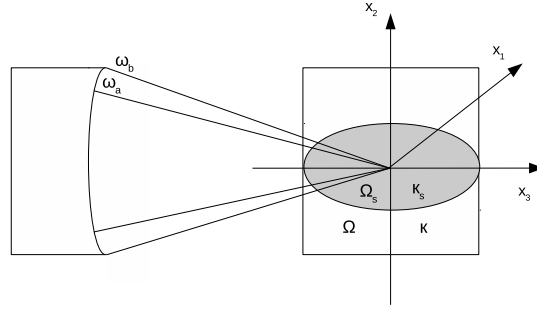


Figure 1: Depiction of problem geometry. Dual-frequencies focused on ellipsoid scatterer. Major axis of ellipsoid located along direction of propagation.

A similar process is applied for the second-order wave equation [6], retaining terms up to the second-order gives,

$$\nabla^2 P_2(\underline{x}, t) - \frac{1}{c_0^2} \frac{\partial^2}{\partial t^2} P_2(\underline{x}, t) = -\frac{(1-\Gamma)}{\rho_0 c_0^4} \frac{\partial^2}{\partial t^2} P_1^2(\underline{x}, t) \quad (4)$$

where the term $\Gamma = 1 + B/A$ contains the nonlinear parameter. The source term $\frac{\partial^2}{\partial t^2} P_1^2(\underline{x}, t)$ describes the interaction of the two first-order waves

that gives rise to several frequency components. Considering $P_1 = \text{Re}(P_{1a} + P_{1b})$, P_1^2 can be expanded as $\text{Re}(P_{1a}^2) + \text{Re}(P_{1b}^2) + \text{Re}(P_{1a}P_{1b}) + \text{Re}(P_{1a}^*P_{1b}) + \frac{1}{2}|P_{1a}| + \frac{1}{2}|P_{1b}|$, where $*$ represents the complex conjugate. The aforementioned terms represent the second harmonic for P_{1a} , the second harmonic for P_{1b} , the sum frequency term, the difference frequency term, and DC component respectively. This analysis deals only with the difference-frequency component arising from the term $\text{Re}(P_{1a}^*P_{1b})$. Converting to the frequency domain and applying Green's Theorem to Eqn. (4), the solution to the second-order field is,

$$P_2(\underline{x}) = k_2^2 \int_{\Omega_s} \frac{(\Gamma - 1)}{\rho_0 c_0^2} P_{1a}^* P_{1b} G(\underline{x}, \underline{x}_0) d\underline{x}_0 \quad (5)$$

where $k_2 = k_b - k_a$ is the difference frequency. The second-order pressure P_2 is considered to be a radiated component. Therefore, for observations \underline{x}_0 within the object, the pressure P_2 will be zero.

3 Computational Method

The first-order scattered fields inside the scattering object are evaluated using Neumann series, an asymptotic series around the gauge parameter ϵ . The procedure is demonstrated for P_{1a} . The solution form is,

$$P_{1a}(\underline{x}) = \sum_{n=0}^N \epsilon^n \phi_n(\underline{x}) \quad (6)$$

The coefficients ϕ_n are obtained by substituting the series (6) into Eqn. (2). Equating like terms of ϵ finds the zeroth-order coefficient ϕ_0 to be the incident pressure and all subsequent terms to be determined recursively from Eqn. (7),

$$\phi_n(\underline{x}) = k_a^2 \int_{\Omega_s} \gamma_\kappa(\underline{x}_0) \phi_{n-1}(\underline{x}_0) G(\underline{x}, \underline{x}_0) dV_0 \quad (7)$$

The Neumann Series approximation is valid for weak scattering where ϵ is small. As ϵ increases, the series diverges due to singularities that can be introduced in the complex ϵ plane. This has been addressed by recasting the Neumann series to a rational function of two polynomials in ϵ . The Neumann series approximation is recast using Padé Approximants [1][2],

$$\phi_0(\underline{x}) + \sum_{n=1}^N \epsilon^n \phi_n(\underline{x}) = \phi_0(\underline{x}) + \frac{\sum_{l=1}^M A_l \epsilon^l}{1 + \sum_{m=1}^M B_m(\underline{x}) \epsilon^m} \quad (8)$$

where $N = 2M + 1$. Equating like terms of ϵ in Eqn. (8), the coefficients A_l and B_m can be found. Once the first-order pressure fields P_{1a} and P_{1b} are determined, the far field second-order field P_2 can be computed from the integral given in Eqn. (5).

4 Results

The results for the difference-frequency are presented for an ellipsoidal shaped scatterer with an aspect ratio of 2. The major-axis of the ellipsoid has a nondimensional length of $a = 1$ and is along the direction of the incident beam. The computation grid of cubic length $2 \times a$ was discretized using a uniform distribution of $N_s = 128$ points. The compressibility spatial function $\gamma_\kappa(\underline{x})$ is 1 inside the volume Ω_s and 0 otherwise. A FFT based quadrature method was applied to Eqn. (7) to determine the Neumann Series coefficients using $N = 15$. An order of $M = 7$ was utilized to ensure convergent Padé Approximant terms.

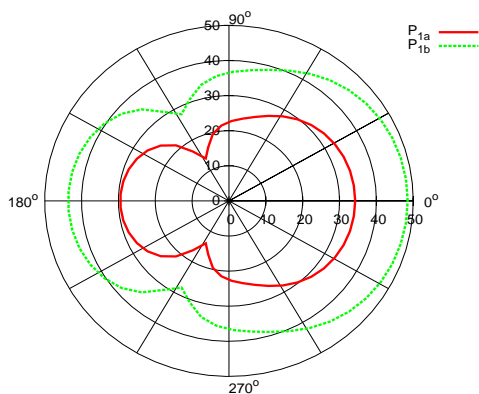


Figure 2: The first-order pressure fields are plotted at a distance of $10 \times a$. A $k_a a = 3.14$ and $k_b a = 3.17$ were considered with a gauge parameter $\epsilon = 1$.

The angular distribution of the scattered pressure produced from the aforementioned method is presented for an observation radius of $10 \times a$. The first-order pressures P_{1a} and P_{1b} are shown in Fig. 2 for an $\epsilon = 1$ with a $k_a a = 3.14$ and $k_b a = 3.17$. The scattered energy appears predominantly in the forward and backward direction as a result of the orientation of the scattering object. The field P_{1b} radiates stronger in comparison to P_{1a} .

The second-order pressure field due to the difference frequency component is evaluated for a nonlinear parameter of $B/A = 6.5$. An analysis was performed comparing the sensitivity of the field due to a varying contrast parameter $\epsilon = 0.25, 0.5, 1.0, 2.0$ shown in Fig. 3. The observable far-field scattering for the difference-frequency appears omnidirectional and of much lower amplitude. Increasing ϵ from 0.25 to 0.5 and 1.0 saw modest increases of about 3 dB respectively. Increasing to a larger contrast $\epsilon = 2.0$ saw an increment of about 10 dB. Varying the contrast did not show any changes in directivity pattern in the difference-frequency field.

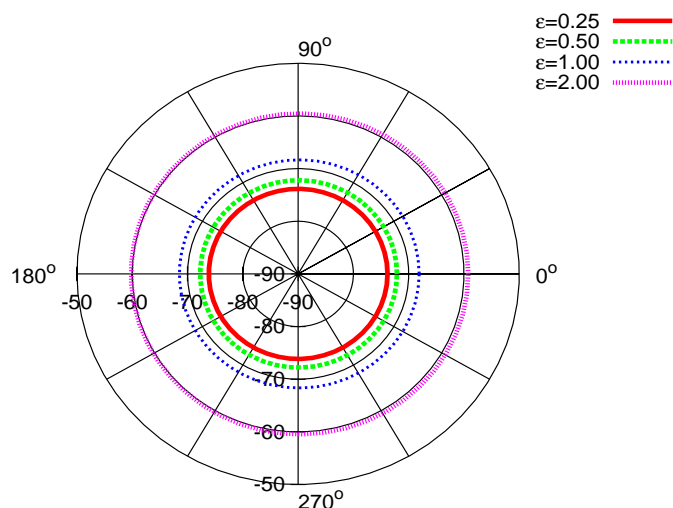


Figure 3: Difference frequency pressure from an ellipsoid at observation of $10 \times a$. Comparison of various ϵ shown.

5 Conclusions

The scattered field produced from the difference-frequency due to the interaction of two incident beams was observed. The first-order pressure fields inside an ellipsoid was calculated using the Neumann Series Approximation. To consider high contrast, the series was recast using Padé Approximants. The field due to the difference frequency increases with compressibility contrast, however has a magnitude that is still quite small.

References

- [1] Bender, C. M. and Orzag, S. A., *Advanced Mathematical Methods for Scientists and Engineers*, McGraw-Hill, Inc, 1978.

- [2] Chandra, K., Isler, S.K., and Thompson, C., "Acoustic scattering in three-dimensional fluid media," *J. Acoust. Soc. Am*, Vol. 98, pp. 3462-3467, 1995.
- [3] Darvennes, C. M. and Hamilton, M. F., "Scattering of sound by sound from two Gaussian beams," *J. Acoust. Soc. Am*, Vol. 87, pp. 1955-1964, 1989.
- [4] Fatemi, M. and Greenleaf, J. F., "Vibroacoustography: An imaging modality based on ultrasound-simulated acoustic emission," *Proc. Natl. Acad. Sci. USA*, Vol. 96, pp. 6603-6608, 1999.
- [5] Ingard, K. U. and Brown, D. C., "Scattering of Sound by Sound," *J. Acoust. Soc. Am*, Vol. 28, pp. 367-369, 1956.
- [6] Morse, P. M. and Ingard, K. U., *Theoretical Acoustics*, McGraw-Hill, Inc, 1986.
- [7] Silva, G. T. and Mitri, F. G., "Difference-frequency generation in vibroacoustography," *Phys. Med. Biol.*, Vol. 56, pp. 5985-5993, 2011.
- [8] Thierman, J., "Sources of Difference Frequency Sound in a Dual-Frequency Imaging System with Implications for Monitoring Thermal Energy," Massachusetts Institute of Technology, 2004.